PERFORMANCE INVESTIGATION OF ANFIS CONTROLLED LLC RESONANT CONVERTER FOR DC TO DC ENERGY CONVERSION

R. ARUL JOSE
Research Scholar, Anna University, Tamil Nadu, India
aruljoser@gmail.com

B. DORA ARUL SELVI
Holy Cross Engineering College, Tuticorin 628 851, Tamil Nadu, India
b.doraarulselvi@gmail.com

Abstract: This paper presents development of a performance analysis of neuro fuzzy controllers to overcome the appearance of nonlinearities and uncertainties in the LLC resonant converter. This paper addresses a LLC resonant converter circuits are built for low output voltages (24 V) and such circuits can be useful for Telecom and server application. For obtaining the DC voltage transfer function Fundamental Harmonic Approximation (FHA) method has been adopted. Important issues of this converter are physical size, high conversion ratio, efficiency, and startup. The proposed topology has energy conversion efficiency of 92%, when operated at fully loaded condition. A neuro fuzzy controller based LLC isolated DC–DC converters are also proposed to regulate over wide range of loads. Switching losses are minimized by zero voltage switching by the use of resonant inductor and capacitor. This converter has advantages like low switching loss, less EMI, and less switching stresses.

Key words: *ANFIS, DC-DC converter, Fundamental Harmonic Approximation (FHA), Pulse Width Modulation (PWM), Series parallel resonant converter (SPRC).*

1. Introduction

In soft switching converters, resonant components are used to create oscillatory voltage or current waveforms so that zero-voltage or zero-current switching conditions could be created for the power switches. Resonant converters are desirable for power conversion due to their reasonably smaller size and lower power losses resulting from high-frequency operation and intrinsic soft switching. Among all the topologies of the resonant converters, the series–parallel resonant converter (SPRC) shares the advantages of both the pure series converter and pure parallel converter [1-6].

The advantage of series resonant converter is that the series resonant capacitors act as a dc blocking capacitor. Hence the converter is used in half bridge arrangements without any additional setup to control unbalance in the power MOSFET switching times and forward voltage drops. The advantage of parallel resonant converter is that it is extremely desirable for applications with short circuit proof. Also in this converter, the current carried by the power MOSFET's and resonant components are relatively independent of load. The series parallel LLC resonant converter combines the above said advantages [9-13]. Taking a look into a switched mode power supply, a rectification stage can be found on the secondary side of the converter which rectifies the rectangular power signal, which is being transferred from the primary side to the secondary side of the SMPS via a transformer and diodes. The well designed LLC resonant converter can realize ZVS for the main switches from no-load to full load, to minimize voltage stress on them[7, 8]. With the rapid development of Telecom technology, industry continues to update the requirements for power supplies. For telecommunication and computing system applications, power supplies require increasing current level while the supply voltage keeps decreasing.

However, it is known that switching DC–DC converters are highly nonlinear systems with parameter uncertainties and variable operating conditions. Conventional controllers generally give overshoot in output voltage and high initial current when the rise time of response is reduced. The conventional control method based on the averaging and linearization techniques will provide poor dynamic performance and even make the system unstable [17]. On the other hand, intelligent controllers, such as ANFIS controller are capable of handling uncertainties and also training and learning from process itself.

The integration of neural network architectures with fuzzy inference system has resulted in a very powerful strategy known as adaptive network-based fuzzy inference system (ANFIS) [12-16]. Some researchers suggest that neural networks and fuzzy control are in fact special instances of adaptive networks. The suggested fuzzy inference system has the advantage that it can not only take linguistic information from human experts but also adapt itself using numerical data to achieve better performance. The developed ANFIS

has the ability to learn about the nonlinear dynamics and external disturbances of the converter with a stable output, small steady error, and fast disturbance rejection.

2. LLC Resonant Converter

Fig.1 shows the proposed concept of LLC resonant converter. The resonant tank consisting of three reactive energy storage elements (LLC) has overcome the conventional resonant converter with two elements. The first stage converts a DC voltage to high frequency AC voltage. The second stage converts AC power to DC power by suitable high frequency rectifier and filter circuit [1-6].

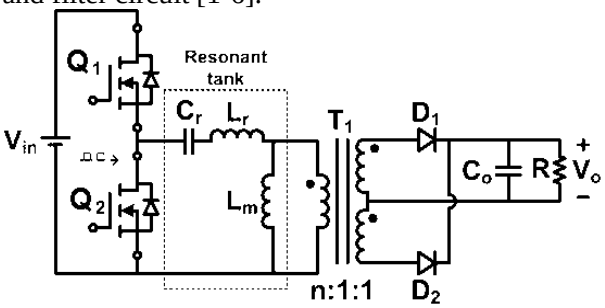

Fig.1. LLC half bridge resonant converter

The proposed LLC resonant converter can realize ZVS for main switches from no load to full load. Generally, the LLC resonant converter consists of a conventional controller with MOSFETs, a resonant network and a rectifier network. The proposed topology uses ANFIS controller to delivers a gate signal with variable duty ratio to two MOSFETs alternatively at constant frequency of load variations to regulate the output voltage, V_{out}, which is called PWM (Pulse width Modulation). The resonant network is comprised of two resonant inductors and one resonant capacitor (LLC). The resonant inductances, L_r and L_m and capacitor, C_r act as a voltage divider whose impedance is varied by the operation frequency so that the desirable output voltage can be obtained, as shown in Equation 1. The rectifier network rectifies sinusoidal waveforms from the resonant network and delivers to the output stage.

3. AC Analysis of the Proposed LLC Series Parallel Resonant Converter

In the ac analysis, the output rectifier and filter are replaced by the equivalent AC resistance and the square-wave input voltage source is replaced by its fundamental sinusoidal equivalent [7]. The power transfer from input to output is assumed to be only via the fundamental component and the contribution of all the harmonics is neglected. The equivalent circuit for LLC series parallel resonant converter is shown in Fig.2. The output power is associated to the output load resistance R_o. R_{ac} is the load resistance reflected to the transformer primary side.

$$n \cdot V_{out} = \frac{R_{ac} \parallel \omega L_m}{1/\omega C_r + \omega L_r + R_{ac} \parallel \omega L_m} \cdot V_{in} \quad (1)$$

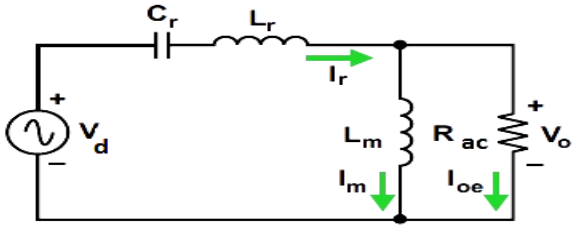

Fig.2. Equivalent circuit for LLC resonant converter

Where V_d is input voltage and R_{ac} is load resistance. Even though the input voltage, V_d is a square waveform controlled by two power MOSFET's, it could also be considered as a sinusoidal alternating waveform by the fundamental approximation. With this approximation, the voltage conversion ratio can be expressed as shown in Equation 2.

$$M = \frac{2n \cdot V_o}{V_{in}} = \frac{\left(\omega/\omega_r\right)^2 \cdot (m-1)}{\sqrt{\left[\left(\omega/\omega_p\right)^2 - 1\right]^2 + \left(\omega/\omega_r\right)^2 \cdot \left[\left(\omega/\omega_r\right)^2 - 1\right]^2 \cdot ((m-1) \cdot Q)^2}} \quad (2)$$

Where, $m = \frac{L_p}{L_r}$, $\omega_r = \frac{1}{\sqrt{L_r C_r}}$, $\omega_p = \frac{1}{\sqrt{L_p C_r}}$, and $Q = \frac{1}{R_{ac}}\sqrt{\frac{L_r}{C_r}}$ and R_{ac} and V_d can be expressed $\frac{8 \cdot n^2 \cdot V_{out}}{\pi^2 \cdot I_{out}}$ and $\frac{V_{in}}{2}$ respectively.

From Equation 2, there are two resonant frequencies. One is ω_p which is determined by (L_m + L_r) and C_r and the other is ω_r which is determined by L_r and C_r. By using this equation, a voltage conversion ratio of the converter, namely gain curve, can be plotted with according to the variation of operating frequency & load as shown in fig. 4. The highest value for each curve is called 'peak gain' and is placed between two resonant frequencies, ω_p and ω_r. As output load increases more and more, a value of the peak gain lessens and the peak gain position moves to a higher frequency. Meanwhile, it can be seen that the resonant gain at ω_r is fixed even though the output load is unbalanced. The gain curve demonstrates that the gain decreases and output voltage reduces when the operating frequency applied to the resonant network increases in the ZVS region.

Series resonant frequency

$$f_o = \frac{1}{2\pi\sqrt{L_r C_r}} \quad (3)$$

Series parallel resonant frequency

$$f_p = \frac{1}{2\pi\sqrt{(L_r + L_m)C_r}} \quad (4)$$

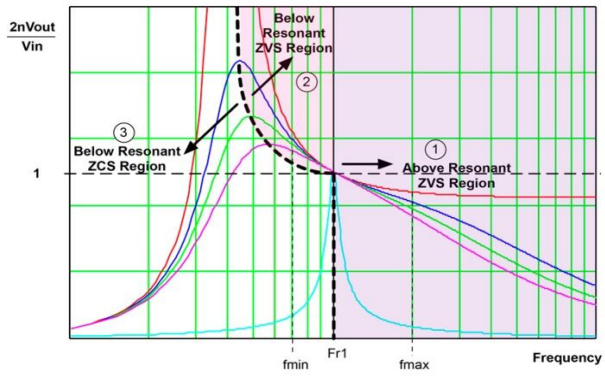

Fig.3.Conversion ratio curve of an LLC resonant converter

The switching frequency is higher than series parallel resonant frequency and lower than series resonant frequency, so that zero voltage switching turn-on can be achieved. Design of transformer turns ratio should satisfy,

$$G_{dc} \le \frac{V_o}{V_{in(Max-dc)/2}} (@ f_{sw} = f_o) \quad (5)$$

$$n \ge \frac{V_{in(Max-dc)}}{2V_o} \quad (6)$$

The determination of Q, k, n and f_s must meet the requirement of DC voltage gain for the full load in case of minimum input voltage. After the determination of Q, k, n and f_{sw}, the values of L_r, C_r and L_m can be calculated.

a. Operation at Resonance:

In this mode the switching frequency is the same as the series resonant frequency. When switch S1 turns off, the resonant current falls to the value of the magnetizing current, and there is no further transfer of power to the secondary side. By delaying the turn-on time of switch S2, the circuit achieves primary-side ZVS and obtains a soft commutation of the rectifier diodes on the secondary side. However, it is obvious that operation at series resonance produces only a single point of operation. To cover both input and output variations, the switching frequency will have to be adjusted away from resonance.

b. Operation below Resonance:

Here the resonant current has fallen to the value of the magnetizing current before the end of the driving pulse width, causing the power transfer to cease even though the magnetizing current continues. Operation below the series resonant frequency can still achieve primary ZVS and obtain the soft commutation of the rectifier diodes on the secondary side.

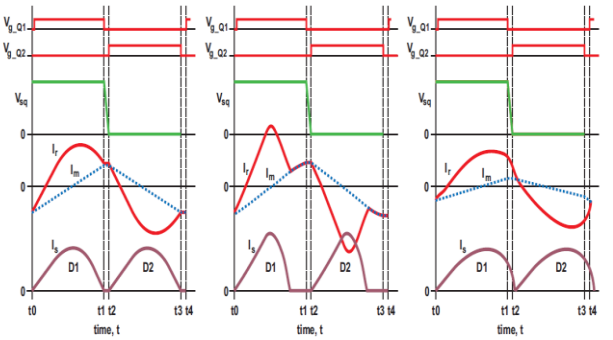

a. At f_o b. Below f_o c. Above f_o

Fig.4. Operation of LLC Resonant Converter

The secondary-side diodes are in discontinuous current mode and require more circulating current in the resonant circuit to deliver the same amount of energy to the load. This additional current results in higher conduction losses in both the primary and the secondary sides. However, one characteristic that should be noted is that the primary ZVS may be lost if the switching frequency becomes too low. This will result in high switching losses and several associated issues.

c. Operation above Resonance:

In this mode the primary side presents a smaller circulating current in the resonant circuit. This reduces conduction loss because the resonant circuit's current is in continuous-current mode, resulting in less RMS current for the same amount of load. The rectifier diodes are not softly commutated and reverse recovery losses exist, but operation above the resonant frequency can still achieve primary ZVS. Operation above the resonant frequency may cause significant frequency increases under light-load conditions. The foregoing discussion has shown that the converter can be designed by using either $f_{sw} \ge f_0$ or $f_{sw} \le f_0$, or by varying f_{sw} on either side around f_0. Further discussion will show that the best operation exists in the vicinity of the series resonant frequency, where the benefits of the LLC converter are maximized.

4. Mathematical Modeling Using State Space Technique

The mathematical modeling using state space technique can be obtained assuming all the components to be ideal. The state space equation for LLC SPRC converter is

$$\frac{di_1(t)}{dt} = \frac{R_{ac}}{L_r} i_2(t) + \frac{V_i(t)}{L_r} - \frac{V_C(t)}{L_r} \quad (7)$$

$$\frac{di_2(t)}{dt} = \frac{L_r + L_m}{L_r L_m} R_{ac} i_2(t) + \frac{V_i(t)}{L_r} - \frac{V_c(t)}{L_r} \quad (8)$$

$$\frac{dV_c(t)}{dt} = \frac{i_1(t)}{C} \quad (9)$$

The state space model of proposed LLC converter is

$$\frac{d}{dt}\begin{bmatrix} i_1(t) \\ i_2(t) \\ V_c(t) \end{bmatrix} = \begin{bmatrix} 0 & \frac{R_{ac}}{L_r} & -\frac{1}{L_r} \\ 0 & \frac{L_r + L_m}{L_r L_m} R_{ac} & -\frac{1}{L_r} \\ \frac{1}{C_r} & 0 & 0 \end{bmatrix} \begin{bmatrix} i_1(t) \\ i_2(t) \\ V_C(t) \end{bmatrix} + \begin{bmatrix} \frac{1}{L_r} \\ \frac{1}{L_r} \\ 0 \end{bmatrix} \begin{bmatrix} V_i(t) \end{bmatrix}$$

(10)

The output equation is

$$\begin{bmatrix} V_o \end{bmatrix} = \begin{bmatrix} 0 & R_{ac} \end{bmatrix} \begin{bmatrix} i_1(t) \\ i_2(t) \end{bmatrix} \quad (11)$$

Design of the PI controller:

An adaptive digital PID controller was designed to compare with the results of ANFIS Controller. The standard equation of a PID controller is

$$u(t) = K_p e(t) + K_i \int e(t)dt + K_d \frac{d}{dt} e(t) \quad (12)$$

System performance depends on the values of the proportional constant K_p, the integral constant K_i and the derivative constant K_d. By descretizing the equation, follows:

$$u[k] = K_p e(k) + K_i T. \sum_{i=0}^{k} e[i] + K_d . \{e[k] - e[k-1]\} \quad (13)$$

u[k]and e[k]are the output and error for the k-th sample consequently. The error e[k]is calculated as follow:

$$e[k] = V_{ref} - ADC[k] \quad (14)$$

where ADC[k] is the converted digital value of the k-th sample of the output voltage, and V_{ref} is the reference digital value of the desired output voltage. For tuning the digital PID controller Ziegler-Nichols technique was used. Ziegler-Nichols formulae for specifying the controllers are based on plant step responses. It is also typical of a plant made up of a series of first order systems. The response is characterized by two parameters, L the delay time and T the time constant.

TYPE	Kp	Ti= Kp/ Ki	Td= Kd/ Kp
P	T/L	∞	0
PI	0.9T/L	L/0.3	0
PID	1.2T/L	2L	0.5L

Table.1. Ziegler-Nichols formulae

These are found by drawing a tangent to the step response at its point of inflection and noting its intersections with the time axis and the steady state value.

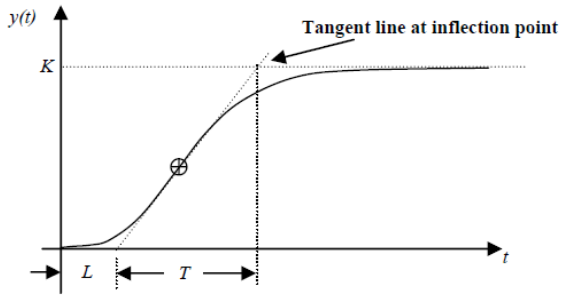

Fig.5. Response curve for Ziegler-Nichols Method

5. ANFIS controller

Adaptive network architecture, ANFIS, and a learning algorithm by which the ANFIS could construct a desired input–output mapping are proposed. The adaptive controller only extract the terminals corresponding to the error and change in error [14]. From these measurements, ANFIS provides a signal relative to a percentage duty cycle signal for a peripheral interface microcontroller that generates the converter actual duty cycle. A control topology is developed and investigated. Both fuzzy logic principles and learning functions of neural networks are employed collectively to construct the adaptive fuzzy network inference system for the control topology. Initially, a basic fuzzy logic controller is set up utilizing linguistic rules. Then, numerical data are used for training the controller. The number of membership functions is chosen seven so as to cover the entire input space. The proposed ANFIS is a multilayer neural network-based fuzzy logic controller. The network architecture is built such that the internal nodes relate to the components of fuzzy controller. The system has a total of five layers. The architecture of the network is shown in Fig. 6.

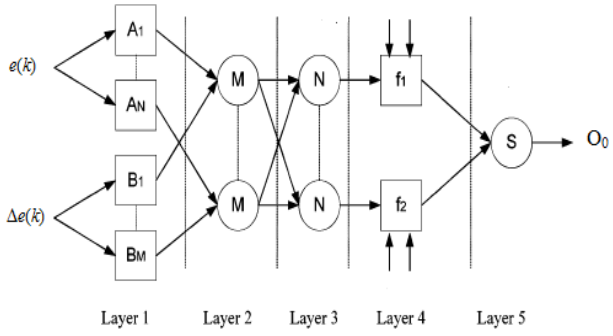

Fig.6. ANFIS structure

Layer 1-Input Layer: This layer is an input node, which corresponds to two input variable. These nodes only bypass input signals to the next layer. The input variables are the output voltage error e(k) = V_{ref} - V_o and the change in voltage error Δe(k) = [e(k) − e(k − 1)], respectively. The fuzzy membership function

proposed for the input variable voltage error e(k) and Δe(k) are negative large (NL), negative medium (NM), negative small (NS), zero (ZE), positive large (PL), positive medium (PM), positive small (PS). The output of the neuron i in layer 1 is obtained as

$$O_i^1 = f_i^1\left(net_i^1\right) = net_i^1 \tag{15}$$

Where net_i^1 is the i_{th} input to the node of layer 1, namely, the error and the change in error.

Layer 2-Input membership layer: This layer acts as a linguistic label of one of the input variables in layer 1. The triangular membership function is chosen for its simplicity. For the change in voltage error Δe(k), the initial values of the premise parameters are chosen so that the membership functions are equally spaced along the operating range of each input variable. The weights between input and membership level are assumed to be unity. The output of neuron j in the second layer can be obtained as follows:

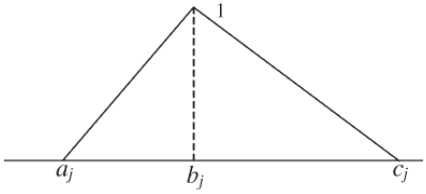

Fig.7. Single membership function

$when(X_i > a_j) and (X_i < b_j)$

$$O_j^2 = f_j^2\left(net_j^2\right) = \frac{\left(X_i - a_j\right)}{\left(b_j - a_j\right)} \tag{16}$$

$else\ when(X_i > b_j) and (X_i < c_j)$

$$O_j^2 = f_j^2\left(net_j^2\right) = \frac{\left(X_i - c_j\right)}{\left(b_j - c_j\right)} \tag{17}$$

where a_j , b_j , and c_j are the corners of the j_{th} membership function in layer 2 and X_i is the i_{th} input variable to the node of layer 2, which could be either the value of the error or the change in error.

Layer 3- Rule Layer: Each node in layer 3 multiplies the incoming signal and outputs the result of the product. The conjunction of the rule antecedents is determined by the fuzzy operation intersection that is implemented by the product operator. Consequently, each node of this layer is a rule node that represents one fuzzy control rule. Each node takes two inputs, one from nodes A_1–A_7 and the other from nodes B_1–B_7 of layer 2. Nodes A_1–A_7 defines the membership values for the voltage error and nodes B_1–B_7 define the membership values for the change in voltage error. Accordingly, there are 49 nodes in layer 3 to form a fuzzy rule base for two input variables, with seven linguistic variables for the input voltage error e(k) and change in voltage error Δe(k). The output of neuron k in layer 3 is obtained as

$$O_k^3 = f_k^3\left(net_k^3\right) = net_k^3 \tag{18}$$

Where

$$net_k^3 = \prod_j w_{jk}^3 y_j^3 \tag{19}$$

and y_j^3 represents the j_{th} input to the node of layer 3 and w_{jk}^3 is assumed to be unity.

Layer 4-output membership Layer: An output membership neuron receives inputs from the fuzzy rule neurons and combines them by using the fuzzy operation union. This was implemented by the maximum function. Layer 4 acts upon the output of layer 3 multiplied by the connecting weights. These link weights represent the output action of the rule nodes evaluated by layer 3. That output is given by

$$O_m^4 = f_m^4\left(net_{km}^4\right) = \max\max\left(net_{km}^4\right) \tag{20}$$

and

$$net_{km}^4 = O_{k\,km}^3 \tag{21}$$

where the count of k depends on the links from layer 3 to the particular m_{th} output in layer 4 and the link weight w_{km} is the output action of the m_{th} output associated with the k_{th} rule. This level is essential in ensuring the system's stability and allowing a smooth control action.

Layer 5 – Defuzzification: Layer 5 is the output layer and acts as a defuzzifier. The single node in this layer takes the output fuzzy sets clipped by the respective incorporated firing strengths and combines them into a single fuzzy set. The output of the neuro-fuzzy system is crisp, and thus a combined output fuzzy set must be defuzzified. The sum–product composition method was used. It calculates the crisp output as the weighted average of the centroids of all output membership functions.

$$O_0 = f_0^4\left(net_0^4\right) = net_0^4 \tag{22}$$

and

$$net_0^5 = \frac{\sum_m O_m^4 a_{Cm} b_{Cm}}{\sum_m \left(O_m^4 b_{Cm}\right)} \tag{23}$$

where a_{Cm} and b_{Cm} for m = 1, . . . , 5 are the centers and widths of the output fuzzy sets, respectively. The values for the b_{Cm}'s were chosen to be unity. This scaled output corresponds to the control signal (percent duty cycle) to be applied to maintain the output voltage at a constant value.

Learning Algorithm: The only weights which are trained are those between layer 3 and layer 4. The

back-propagation network is used to train the weights of this layer. The weights of the neural network were trained offline before they were used in the experimental setup. The learning algorithm used can be described in the following steps.

Step 1: Calculate the error for the change in the control signal (duty cycle) based on the type of the converter, i.e.,

$$E_0 = T_0 - O_0^5 \tag{24}$$

where E_o, T_o, and O_0^5 are the output error, the target control signal, and the actual control signal, respectively.

Step 2: Calculate the error gradient, i.e.,

$$\delta_m = E_0 \times f'\left(O_1^4, \ldots, O_m^4\right) \tag{25}$$

where

$$f\left(O_1^4, \ldots, O_m^4\right) = \frac{\sum_{j=1}^{m} O_j^4 a_{Cj}}{\sum_{j=1}^{m} O_j^4} \tag{26}$$

and the partial derivative of f with respect to O_m^4 is given by

$$f'_{O_m^4}(O_1^4, ,, , , , O_m^4) = \frac{\sum_{\substack{j=1 \\ j \neq m}}^{m-1} O_j^4 (a_{Cm} - a_{Cj})}{\left(\sum_{j=1}^{m} O_j^4\right)^2} \tag{27}$$

where a_{Ci} for i = 1, . . . , 5 are the centers of the output fuzzy sets and O_j^4 is the firing strength from node j in layer 4.

Step 3: Calculate the weight correction

$$\Delta_{w_{km}} = \eta \delta_m O_k^3 \tag{28}$$

to increase the learning rate. The Sejnowski–Rosenberg updating mechanism was used, which takes into account the effect of past weight changes on the current direction of the movement in the weight space. This is given by

$$\Delta_{w_{km}}(t) = \eta(1-\alpha)\delta_m O_m^3 + \alpha \Delta_{w_{km}}(t-1) \tag{29}$$

where α is a smoothing coefficient in the range of 0–1.0 and η is the learning rate.

Step 4: Update the weights

$$w_{km}(t+1) = w_{km}(t) + \Delta_{w_{km}}(t) \tag{30}$$

where t is the iteration number. The weights linking the rule layer (layer 3) and the output membership layer (layer 4) are trained to capture the system dynamics and therefore minimize the ripples around the operating point.

6. DESIGN AND RESULTS

For the design of LLC resonant converter, the values of all elements were obtained using design procedure to assure resonance for almost different power ranges and also to limit the current and voltage peak values. In this section, a design procedure is proposed. A transformer with center tapped secondary side is used and input voltage is supplied from power factor correction pre-regulator. A DC/DC converter with 192W/24V output has been selected as a design example.

The design specifications are as follows:

- Nominal input voltage: 400V DC
- Output: 24V/8A (192W)
- Hold-up time requirement: 20ms
- DC link capacitor: 220Mf

Parameters	Design values
Normal Input AC voltage	280V
Normal DC bulk voltage	400V
Normal output full load	24V/8A
Switching frequency	100kHz @ 24V/8A and 400V DC input
Minimum frequency	78KHz
L_p	630µH
L_r	126µH
C_r	20nH
f_o	100KHz
m	5
Q	0.4
M@f_o	1.12

Table.2. Design Parameter

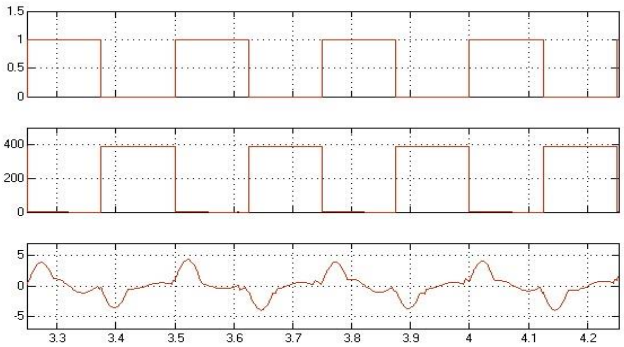

Fig.8. Gate pulse signal, Drain voltage and drain current at half load condition

In high-performance telecommunication applications, the system operation speed, integration density as well as power level requirement continue to increase, resulting in decreased supply voltage and increased supply current. High-power-density power conversion is also demanded for telecommunication applications [18]. High switching frequency of 78 KHz to 100 KHz is used to improve power density, and this

topology features high efficiency at high switching frequency. The figure shows the experimental waveforms at full load. The smooth rising edge of gate source voltage proves that the LLC converter achieves ZVS.

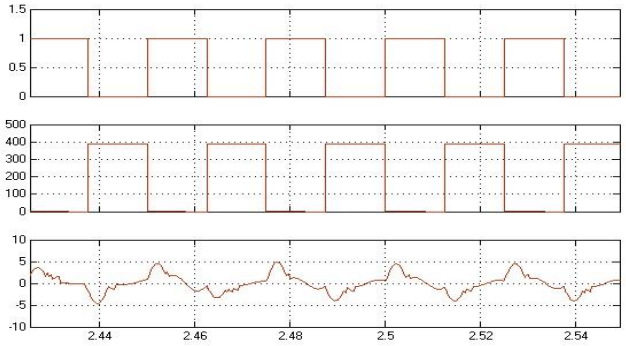

Fig.9. Gate pulse signal, Drain voltage and drain current at full load condition

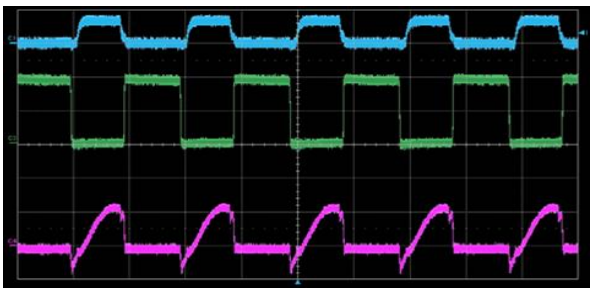

Fig.10. Gate pulse signal, Drain voltage and drain current at Full load condition

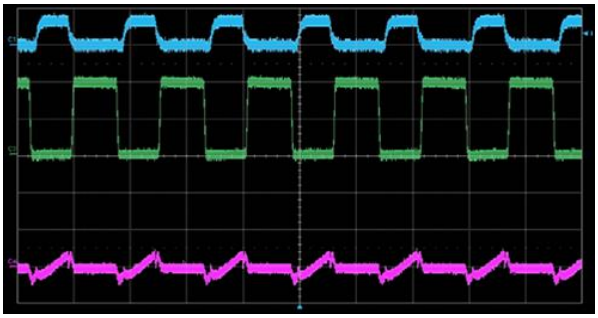

Fig.11.Gate pulse signal, Drain voltage and drain current at no load condition

A PID controller was designed to maintain output DC voltage at desired fixed value against each distortion in output load.

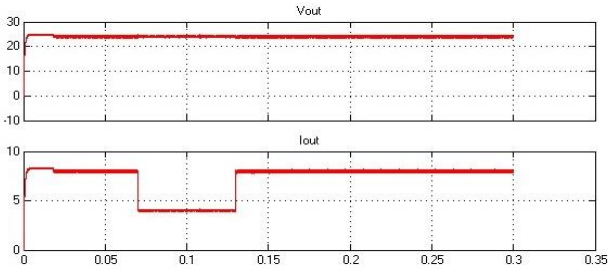

Fig.12. Voltage and Current waveform for PID Controller

Simulation of output voltage response versus load condition variation is shown in Fig.13. As it can be seen in the figure, settling time of voltage for raising edge was about 18.5ms. Also, output voltage distortions were about 1.1 V (4.58 %).

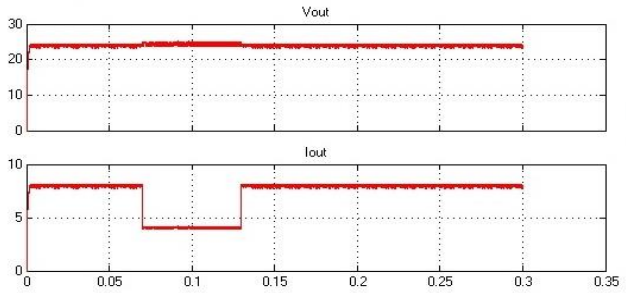

Fig.13. Voltage and Current waveform for Neuro Fuzzy Controller

ANFIS has a network-type structure similar to that of a neural network which maps inputs through input membership functions and associated parameters, and then through output membership functions and associated parameters to outputs, can be used to interpret the input-output map. The parameters associated with the membership functions will change through the learning process. The computation of these parameters is facilitated by a gradient vector, which provides a measure of how well the fuzzy inference system is modeling the input/output data for a given set of parameters. Based on the 72001 training data set, ANFIS simulation program automatically generates a second-order Sugeno fuzzy type, using 7 triangular membership functions and 49 rules. The settling time of voltage for raising edge was about 2.5ms. Also the output voltage distortion is 0.6 V (2.5 %) with a small overshoot of 1.833%.

	Settling Time (ms)	**Ripple Voltage (V)**	**Peak Overshoot (%)**
PID Controller	18.5	1.1	4.167
ANFIS Controller	2.5	0.6	1.833

Table.3. Comparison of PID and Neuro-Fuzzy Controller

The intelligent ANFIS controller behaves effectively like an adaptive local tuned controller designed for each operating point and gives an improved performance compared to the conventional controller.

CONCLUSION

The LLC resonant converter has Smaller switching losses and wide input range operation and makes converter attractive as front-end AC/DC converters. In this paper, based on a theoretical analysis

of circuit operation at the peak gain point, a precise analytical solution for the peak gain has been presented. By using the developed precise analytical solution for the peak gain, it is possible to accurately optimize the resonant tank of a LLC resonant converter, which can regulate output voltage during hold up time. By means of the equivalent circuit generated by the modification FHA analysis, components stress and soft-switching conditions could be found without solving complicated differential equations. With a proper design based on the FHA analysis results, this converter is proved to be able to maintain ZVS operation for all switches with variation of output voltage for the whole range of load level. The resonant converter uses leakage and stray components as the resonant network, so the leakage energy can be transferred to the output stage. The results provide load independent operation and this is a good technique for low voltage applications with wide range of load.

References

1. Xiaodong Li"*A LLC type Dual bridge resonant converter: analysis, design, simulation, and Experimental Results"*, IEEE Trans. Power Electron, IEEE Trans. Power Electron,Vol.29,No.8,August 2014,pp 4313-4321
2. Shih-Yu Chen, Zhu Rong Li, Chern-Lin Chen" *Analysis and Design of Single –stage AC/DC LLC Resonant Converter"*, IEEE Trans. IndustryElectron,Vol.59,No.3,March 2012, pp 1538-1544
3. Yu Fang, Dehong Xu, Yanjun Zhang, Fengchuan Gao, Lihong Zhu," *Design of High Power Density LLC Resonant Converter with Extra Wide Input Range*", IEEE 2007,pp976-981.
4. Sung-Soo Hong, Sang-Ho Cho, Chung-Wook Roh, and Sang-Kyoo Han "*Precise Analytical Solution for the Peak Gain of LLC Resonant Converters*," Journal of Power Electronics, Vol. 10, No. 6,pages 680-685, November 2010
5. A. K. S. Bhat, "*Analysis and design of a series-parallel resonant converter with capacitive output filter*," IEEE Transactions on Industry Applications, vol. 27, no. 3, pages 523-530, May 1991.
6. B. C. Kim, K. B. Park, C. E. Kim, B. H. Lee, and G. W. Moon, "*LLC resonant converter with adaptive link-voltage variation for a high power density adapter*," IEEE Trans. Ind. Electron., vol. 25, no. 9, pp. 2248–2252, Sep. 2010.
7. ST Microelectronics, Application Note "*LLC Resonant Half-Bridge Converter Design Guideline*," Mar. 2007.
8. Fairchild Semi conductor, Application Note "*Half bridge LLC Resonant Converter Design using FSFR-series Fairchild power switch*," September 2007.
9. R. A. Fisher, C. S. Korman, G. A. Franz, G. W. Ludwig, J. P. Walden, S. A. El-Hamamsy, K. Shenai, and M. Kuo, "*Performance of low loss synchronous rectifiers in a series-parallel resonant DC-DC converter*," in Proc. 4th Annu. IEEE Appl. Power Electron. Conf., 1989, pp. 240-246.
10. B. Yang, F. C. Lee, A. J. Zhang, and G. Huang, " *LLC resonant converter for front end DC/DC conversion*," in Proc. 17th Annu. IEEE Appl. Power Electron. Conf., 2002, pp. 1108-1112.
11. D. Fu, B. Lu, and F. C. Lee, "*1 MHz high efficiency LLC resonant converters with synchronous rectifier*," in Proc. IEEE Power Electron. Spec. Conf., 2007, pp. 2404-2410.
12. H.S. Choi, "*Design consideration of half bridge LLC resonant converter*," Journal. of Power Electronics, vol. 7, no. 1, pp. 13-20, Jan.2007
13. L. Robert and A. Steigerwald, "*A Comparison of Half-bridge resonant converter topologies*," IEEE Transactions on Power Electronics, Vol. 3, No. 2, April 1988.
14. Rong-jong Wai, Li-Chung Shih" *Adaptive Fuzzy Neural Network Design for Voltage tracking control of a DC-DC Boost Converter"*, IEEE Trans. Power Electron,Vol.27,No.4,April 2012,pp 2104-2115
15. Kuo-Hsiang Cheng, Chun-fei Hsu, Chih-Min Lin, Tsu-Tian Lee, Chunshien Li*," Fuzzy Neural Sliding-Mode Control for DC-DC Converters Using Asymmetric Gaussian Membership Functions*" IEEE Trans. Industry Electron,Vol.54,No.3,June 2007,pp 1528-1536
16. F. A. Alturki and A. Abdennour, "*Design and simplification of adaptive neuro-fuzzy inference controllers for power plants*," Elect. Power Energy Syst., vol. 21, pp. 465–474, 1999.
17. Ahmed Rubaai, Abdul R.ofoli, Legand Burge, Moses Garuba"*Hardware implementation of an adaptive Network based fuzzy controller for DC-DC Converters"*, IEEE Trans. Industry Electron,Viol.41,No.6,Nov 2005,pp 1557-1565.
18. J. Shing and R. Jang, "*ANFIS: Adaptive network-based fuzzy inference system*," IEEE Trans. Syst., Man Cybern., vol. 23, no. 3, pp. 665–685, May/Jun. 1993
19. J. Alvarez-Ramirez, I. Cervantes, G. Espinosa-Perez, P. Maya, and A. Morales, "*A stable design of PI control for DC–DC converters with an RHS zero*," IEEE Trans. Circuits Syst. I, Fundam. Theory Appl., vol. 48, no. 1, pp. 103–106, Jan. 2001.
20. Juergen Biela, Member, IEEE, Uwe Badstuebner, Student Member, IEEE, and Johann W. Kolar, Senior Member, IEEE," *Impact of Power Density Maximization on Efficiency of DC–DC Converter Systems*", IEEE Trans. Power Electron, vol. 24, no. 1, jan. 2009, pp288-300.